

Antikaon Production in Proton-Nucleus Reactions and the K^- properties in nuclear matter*

A. Sibirtsev[†] and W. Cassing
Institut für Theoretische Physik, Universität Giessen
D-35392 Giessen, Germany

June 24, 2018

Abstract

We calculate the momentum-dependent potentials for K^+ and K^- mesons in a dispersion approach at nuclear density ρ_0 using the information from the vacuum K^+N and K^-N scattering amplitudes, however, leaving out the resonance contributions for the in-medium analysis. Whereas the K^+ potential is found to be repulsive ($\approx +30$ MeV) and to show only a moderate momentum dependence, the K^- selfenergy at normal nuclear matter density turns out to be ≈ -200 MeV at zero momentum in line with kaon atomic data, however, decreases rapidly in magnitude for higher momenta. The antikaon production in $p + A$ reactions is calculated within a coupled transport approach and compared to the data at KEK including different assumptions for the antikaon potentials. Furthermore, detailed predictions are made for $p + {}^{12}\text{C}$ and $p + {}^{207}\text{Pb}$ reactions at 2.5 GeV in order to determine the momentum dependent antikaon potential experimentally.

PACS: 24.10.-i; 24.30.-v; 24.50.+g; 25.40.-h

Keywords: scattering amplitude, dispersion relation, elementary cross section, medium mass modification, antikaon production

1 Introduction

One of the most exciting ideas regarding the hadron properties in nuclear matter is the modification of their mass or energy as a result of their interactions with the nuclear

*Supported by Forschungszentrum Jülich

[†]On leave from the Institute of Theoretical and Experimental Physics, 117259 Moscow, Russia.

environment or a partial restoration of chiral symmetry. According to effective chiral Lagrangians the in-medium antikaon mass should be substantially reduced while the kaon mass is expected to be slightly enhanced [1, 2, 3, 4]. The experimental studies for kaonic atoms [5] indicated that even at normal nuclear density the K^- -mass might decrease by $\simeq 200$ MeV which would imply kaon condensation at 2-3 ρ_0 . The attractive antikaon potentials also have a strong impact on subthreshold K^- production. Indeed, a dropping of the in-medium hadron mass shifts the production threshold to lower energies which leads to an enhanced production yield.

Antikaon enhancement in nucleus-nucleus collisions has been seen in GSI experiments [6, 7, 8] on strangeness production. The dynamical studies performed in Refs. [9, 10, 11, 12] indicate that a dropping of the K^- mass by $\simeq 100 - 120$ MeV (at nuclear saturation density) is necessary to explain the K^- production data for $Ni + Ni$ at 1.6 and 1.85 A·GeV. These potentials are roughly half of those found for kaonic atoms in [5]. Note that the experiments with kaonic atoms investigate stopped K^- -mesons while in the heavy-ion collisions at GSI antikaons with momenta from 300 - 800 MeV/c (relative to the baryonic fireball) are probed. Thus the measurements might be compatible if the antikaon potential would show up strongly momentum dependent. On the other hand, in nucleus-nucleus collisions a complex dynamical time evolution of the system is involved and explicit momentum-dependent potentials cannot be extracted from a comparison of calculations to the experimental data. It is thus desirable to obtain information about the K^+ and K^- potentials under circumstances where the dynamics are much better under control and where the momentum dependence can be studied explicitly. This should be the case for proton-nucleus reactions; here, first transport calculations with antikaon potentials have been presented in Ref. [13].

The in-medium K^- -nucleon scattering amplitude and K^- -mesons mass in nuclear matter in the presence of the $\Lambda(1405)$ resonance was studied in Refs. [14, 15, 16]. We note that the $\Lambda(1405)$ resonance amplitude fits the K^-N scattering for low antikaon momenta relative to the baryonic matter ($p_K \leq 300$ MeV/c) as will also be shown in the following. Furthermore, the K^+ -nucleon scattering amplitude has been investigated experimentally in nuclei by measurements of the elastic and inelastic scattering of kaons on ${}^6\text{Li}$ and ${}^{12}\text{C}$ in Ref. [17].

In this work we investigate more systematically the momentum dependence of the K^+ and K^- potentials at finite nuclear density and its relevance for strangeness production in proton-nucleus reactions. We start in Section 2 with a reminder of the elementary production cross sections from pN and πN production channels and evaluate the K^+ and K^- potentials in a dispersion approach in Section 3. Detailed calculations for antikaon spectra are presented in Section 4 in comparison to the scarce data taken at KEK [18]. Section 5, furthermore, contains our predictions for antikaon spectra at 2.5 GeV on ${}^{12}\text{C}$ and ${}^{208}\text{Pb}$ targets, which can be measured experimentally at COSY, whereas Section 6 concludes this study with a summary and discussion of open questions.

2 Elementary K^- production cross sections

The calculations on strangeness production from either proton-nucleus or heavy-ion collisions are very sensitive to the input for the elementary processes. In case of $p + A$ reactions these important ingredients are the $\pi N \rightarrow K^- X$ and $pN \rightarrow K^- X$ channels as well as a selfconsistent description of the K^- -meson propagation in the residual target nucleus due to the very strong K^- -nucleon final state interaction.

Recently, the exclusive antikaon production from both πN and NN collisions has been analyzed in terms of the One-Boson-Exchange-Model (OBEM) [19]; it was found that the available experimental data for the $\pi N \rightarrow NK\bar{K}$ reaction can be reasonably fitted by a K^* exchange model. In the latter work the average $\pi N \rightarrow NKK^-$ cross section has been parameterized as

$$\bar{\sigma}(\pi N \rightarrow NKK^-) = 1.6815 \left(1 - \frac{s_0}{s}\right)^{1.86} \left(\frac{s_0}{s}\right)^2, \quad (1)$$

where the cross section is given in mb , s is the squared invariant energy and $\sqrt{s_0} = m_N + 2m_K$, with m_N and m_K denoting the masses of the nucleon and kaon, respectively. The relations between the different isotopic channels of the reaction $\pi N \rightarrow NK\bar{K}$ are explicitly given in Ref. [19]. The average cross section (1) is shown in Fig. 1 by the dashed line together with the experimental data [20] corrected by the isospin factors from Ref. [19]. The data are shown as a function of the excess energy $\epsilon = \sqrt{s} - \sqrt{s_0}$ above the reaction threshold and are well reproduced by the parameterization (1).

Note that at excess energies above the π -meson mass reactions channels with additional pions become possible which have to be taken into account for the inclusive K^- -meson production. At excess energies of about 2 GeV the inclusive K^- production cross section (open squares) is about an order of magnitude higher than the exclusive one (full dots). In order to match the inclusive cross section at high energies we adopt the Lund-String-Model (LSM) [21]. The calculated cross section for the reaction $\pi N \rightarrow K^- X$ from the LSM is shown by the triangles in Fig. 1. Experimental data are available for the $\pi^- p \rightarrow K^+ K^- X$ and $\pi^+ p \rightarrow K\bar{K} X$ partial cross sections [20], which can be related to the inclusive K^- -meson production cross section via isospin symmetry as (see also Ref. [22]):

$$\sigma(\pi N \rightarrow K^- X) = 2\sigma(\pi N \rightarrow K^+ K^- X) = \frac{1}{2}\sigma(\pi N \rightarrow K\bar{K} X). \quad (2)$$

These inclusive cross sections (open and full squares in Fig. 1) are below the LSM calculations within a factor of 1.5 - 2. Note, however, that reactions with antihyperons, i.e. $\pi N \rightarrow \bar{Y} K^- X$, also contribute to the inclusive antikaon production at excess energies $\sqrt{s} - m_N - 2m_K > 1.6$ GeV, which are taken into account in the LSM.

The solid line in Fig. 1 illustrates our parameterization for the inclusive $\pi N \rightarrow K^- X$ cross section:

$$\bar{\sigma}(\pi N \rightarrow K^- X) = 1.45 \left(1 - \frac{s_0}{s}\right)^2 \left(\frac{s}{s_0}\right)^{0.26} \quad (3)$$

where the cross section is given in mb and $s_0 = 3.709$ GeV².

The cross section for the $NN \rightarrow NNK\bar{K}$ reaction, with N being either a proton or neutron, $K = K^+$ or K^0 and $\bar{K} = K^-$ or \bar{K}^0 , has been calculated within the

OBEM taking into account both pion and kaon exchange [19]. The isospin averaged $pN \rightarrow NNK\bar{K}^-$ cross section is shown by the dashed line in Fig. 2 together with the available experimental data for the $pp \rightarrow ppK^0\bar{K}^0$ and $pp \rightarrow pnK^+\bar{K}^0$ reactions [20]. The full dots in Fig. 2 show the cross sections for the inclusive K^- -meson production from pp collisions [20, 23]. The triangles represent the results from the LSM, which are well in line with the experimental data at high energies. The single data point at an excess energy of $\simeq 0.1$ GeV falls out of the systematics and violates severely a scaling with 4-body phase space at low excess energies.

The solid line in Fig. 2 shows our parameterization for the inclusive $pN \rightarrow K^-X$ cross section:

$$\bar{\sigma}(pN \rightarrow K^-X) = 0.3 \left(1 - \frac{s_0}{s}\right)^3 \left(\frac{s}{s_0}\right)^{0.9} \quad (4)$$

with the cross section given in mb and $s_0 = 8.19 \text{ GeV}^2$.

In order to propagate the antikaons through nuclear matter we account for the elastic and inelastic K^-N processes and implement the corresponding cross section from the compilation of experimental data [20]. Since the elastic and inelastic cross sections with nucleons are rather well known, antikaon rescattering and absorption is expected to be well under control. For an explicit representation of these cross sections we refer the reader to Ref. [10].

3 Dispersion approach for kaon and antikaon potentials

Due to strangeness conservation the \bar{K} -meson production is associated with K -production¹ and we have to account for the in-medium modifications of both, kaons and antikaons. Furthermore, to study the K^- -momentum spectra from pA collisions one has to evaluate the density as well as the momentum dependence of the K^\pm potentials in nuclear matter.

As pointed out by Brown [24] the study of kaonic atoms indicates a decrease of the K^- mass by $200 \pm 20 \text{ MeV}$ [5], while the experiments at GSI suggest that it is sufficient to drop the antikaon mass at normal baryon density ρ_0 by $\simeq 100\text{-}120 \text{ MeV}$ [10, 11]. This conflicting results might be explained when assuming that the K^- potential or selfenergy depends on the antikaon momentum p_K relative to the nuclear matter. Indeed, the investigations with the kaonic atoms deal with antikaons practically at rest whereas the studies at GSI probe the K^- -mesons with $300 \leq p_K \leq 600 \text{ MeV}/c$ in the nucleus-nucleus cms.

For a first order estimate of the kaon and antikaon potentials we use the low density approximation and express the K and \bar{K} -potential as a function of the baryon density ρ_B and the K^\pm -momentum p_K relative to the nuclear matter rest frame as

$$\Pi^\pm(\rho_B, p_K) = -4\pi \rho_B \text{Re}f^\pm(p_K), \quad (5)$$

where $\text{Re}f^\pm$ is the real part of the K^+N or K^-N scattering amplitude.

¹Fig. 1 indicates that at high energies also antihyperons might be produced instead of kaons.

The relation between the K^+N and K^-N scattering amplitudes is given by the crossing symmetry

$$f^\pm(\omega) = f^{\mp*}(-\omega) \quad (6)$$

and the forward scattering amplitude in the laboratory can be written as

$$f^\pm(\omega) = D^\pm(\omega) + iA^\pm(\omega), \quad (7)$$

with $\omega = \sqrt{p_K^2 + m_K^2}$, where p_K and m_K are the laboratory momentum and kaon mass, respectively, while the imaginary and real part of the amplitude are related by the dispersion relation.

Note that the difficulty in the calculation of the real part for the forward scattering amplitude by dispersion relations comes from the large unphysical cut in the K^-N scattering amplitude and from the available data on the total cross sections in the physical region.

With the subtraction point at $\omega = 0$ the real part of the $K^\pm N$ amplitude may be written in the form [25, 26]

$$D^\pm = D(0) \mp R_Y^\pm(\omega) + \{I^\pm(\omega < m_K) + I^\pm(\omega > m_K)\}. \quad (8)$$

The second term in (8) stems from the contribution from Λ and Σ poles [27],

$$R_Y^\pm(\omega) = \frac{\omega}{16\pi m_N^2} \left(\frac{g_{N\Lambda K}^2 [m_K^2 - (m_\Lambda - m_N)^2]}{\omega_\Lambda (\omega \pm \omega_\Lambda)} + \frac{g_{N\Sigma K}^2 [m_K^2 - (m_\Sigma - m_N)^2]}{\omega_\Sigma (\omega \pm \omega_\Sigma)} \right), \quad (9)$$

where m_N , m_Λ and m_Σ stand for the nucleon, Λ and Σ -hyperon masses, respectively. $g_{N\Lambda K}^2$ and $g_{N\Sigma K}^2$ are the coupling constants, while the kaon energy ω_Y corresponds to the process $Y \leftrightarrow K^-N$, i.e.

$$\omega_Y = \frac{m_Y^2 - m_N^2 - m_K^2}{2m_N}. \quad (10)$$

As was proposed by Bailon et al. [28] and Hendrick and Lautrup [29], rather than to determine both coupling constants it is sufficient to use the effective coupling constant

$$g^2 = \frac{1}{4\pi} \left(g_{N\Lambda K}^2 + g_{N\Sigma K}^2 \frac{m_K^2 - (m_\Sigma - m_N)^2}{m_K^2 - (m_\Lambda - m_N)^2} \right) \quad (11)$$

and approximate the Λ - and Σ -poles by a single pole located between the two, i.e. replacing Eq. (9) by

$$R_Y^\pm(\omega) = g^2 \frac{\omega}{\omega_Y (\omega \pm \omega_Y)} \frac{m_K^2 - (m_\Lambda - m_N)^2}{4m_N^2} \quad (12)$$

with $\omega_Y = 0.11$ GeV.

In Eq. (8) the third term represents the integral contribution from both the unphysical $\omega < m_K$ [30] and the physical region $\omega > m_K$. The amplitude from the unphysical region can be obtained from the low energy solution of Kim [31] or A.D. Martin [32] as

$$I^\pm(\omega < m_K) = \mp \frac{\omega}{\pi m_N} \int_{\omega_{\Lambda\pi}}^{m_K} \frac{d\omega' (m_N^2 + m_K^2 + 2m_N\omega')^{1/2}}{\omega' (\omega' \pm \omega)} A^-(\omega') \quad (13)$$

where $\omega_{\Lambda\pi}$ is the kaon energy corresponding to the $K^-N \rightarrow \Lambda\pi$ reaction threshold,

$$\omega_{\Lambda\pi} = \frac{(m_\lambda + m_\pi)^2 - m_N^2 - m_K^2}{2m_N}, \quad (14)$$

and A^- denotes the imaginary part of the K^-N forward scattering amplitude.

The contribution from the $\pi^0\Lambda$ energy up to the threshold for K^-p elastic scattering stems from two resonances: the $\Sigma(1385)$, which couples to the $\pi\Lambda$ ($88 \pm 2\%$) and $\pi\Sigma$ ($12 \pm 2\%$) channels, and the $\Lambda(1405)$ that decays entirely through the $\pi\Sigma$ channel. A recent review on the phenomenological extrapolation of the K^-N scattering amplitude below the threshold is given in Refs. [33, 34].

In the present calculations we adopt the effective range approximation and express the s -wave amplitude as

$$A^-(\omega) = \frac{0.5 b_0}{(1 + a_0 q)^2 + b_0^2 q^2} + \frac{0.5 b_1}{(1 + a_1 q)^2 + b_1^2 q^2}, \quad (15)$$

where q is the imaginary kaon momentum in the KN center-of-mass system,

$$q^2 = \frac{m_N^2(m_K^2 - \omega^2)}{m_N^2 + m_K^2 + 2m_N\omega}, \quad (16)$$

and the complex scattering lengths $a_j + ib_j$ are taken from the solution of Kim [31]. The first term in Eq. (15) is the cut-off at the $\pi\Sigma$ threshold while the second term is that at the $\pi\Lambda$ threshold.

The contribution from the physical region is calculated as

$$I^\pm(\omega > m_K) = \frac{\omega}{4\pi^2} P \int_{m_K}^{\infty} \frac{d\omega' \sqrt{\omega'^2 - m_K^2}}{\omega'} \left[\frac{\sigma^\pm(\omega')}{\omega' - \omega} - \frac{\sigma^\mp(\omega')}{\omega' + \omega} \right], \quad (17)$$

where σ^\pm stands for the total K^+N and K^-N cross section. In the following we will calculate the K^+p and K^-p amplitudes ² using the cross sections $\sigma^\pm(\omega)$ parameterized as described in the Appendix.

Fig. 3 shows the real part of the forward K^-p scattering amplitude calculated by Eq. (8) together with the experimental results collected by Dumbrais, Dumbrais and Queen [35]. Note that the sign of the real part of the forward scattering amplitude is undetermined experimentally in most cases, but can be fixed from the analysis of the dispersion relations [36, 37]. We find a quite reasonable agreement between our dispersion calculations and the data up to very high kaon momenta. The real part of the K^+p amplitude is shown in Fig. 4 correspondingly. Note that dispersion calculations systematically disagree with the data for kaon momenta above 5 GeV/c.

At low energy the K^-p interaction in vacuum is repulsive due to the coupling to the $\Lambda(1405)$ resonance. However, the observations of kaonic atoms [5] show that

²Actually it is quite difficult to calculate the K^-n and K^+n amplitude since there are no experimental data on the relevant total cross sections at low energies [20] as well as the information about the unphysical cut in K^-n scattering, which complicates the determination of the coupling constants and the subtraction [29].

the real part of the K^- optical potential in nuclear matter is attractive. Indeed, if the $\Lambda(1405)$ is a quasibound state of the $\bar{K}N$ system, then it should dissolve in the medium due to the Pauli blocking of the proton in the $\Lambda(1405)$. A recent analysis of the low energy $\bar{K}N$ interaction in baryonic matter has been performed by Waas, Rho and Weise [14] and the in-medium properties of the $\Lambda(1405)$ resonance were investigated by Ohnishi, Nara and Koch [15]. Both investigations show an attractive $\bar{K}N$ interaction at nuclear matter density. Furthermore, the mean-field approach of Brown and Rho [38] accordingly assumes that in nuclear matter the $\Lambda(1405)$ resonance is insignificant and has no relevance at nuclear densities. We thus also neglect the low energy solution (13) and simply drop the contribution from both $\Sigma(1385)$ and $\Lambda(1405)$ resonances.

It is convenient to write the modification of the K^\pm -meson energy in the medium in terms of a potential U^\pm via

$$U^\pm = -\frac{2\pi}{m_K} \rho_B \text{Re}f^\pm, \quad (18)$$

where ρ_B is the baryon density and m_K the bare kaon mass.

Fig. 5 illustrates our calculations for the potential (18) at nuclear saturation density $\rho_B = \rho_0 = 0.17 \text{ fm}^{-3}$ as a function of the antikaon momentum. The dashed line indicates the result obtained with the total free K^-p scattering amplitude while the fat solid line shows our calculations when excluding the repulsive low energy resonance contribution in the scattering amplitude. The lined area demonstrates the uncertainties due to input parameters. In Fig. 5 we also show the antikaon potential as obtained from the analysis of kaonic atoms from Friedman, Gal and Batty [5], which indicates a lowering of the effective in-medium \bar{K} mass by $200 \pm 20 \text{ MeV}$ at zero antikaon momentum. The crossed rectangle in Fig. 5 shows the antikaon potential (at ρ_0) as implemented in the calculations in Ref. [10] and Li et al. [11]. The latter potentials have been extracted from the experimental data on K^- production at $\theta_{lab} = 0^\circ$ from $Ni + Ni$ collisions at 1.66 and 1.85 A·GeV [6].

Note that our result scales the K^- mass in nuclear matter (at zero momentum) as

$$m_{K^-}^* = m_K (1 - \alpha_K \rho_B/\rho_0) \quad (19)$$

with $\alpha_K \approx 0.2 - 0.22$ roughly in line with the suggestion by Brown and Rho [4] and with the recent calculations by Tsushima et al. [39] within the quark-meson coupling model that predicts a decrease of the K^- -meson mass in nuclear matter at ρ_0 and at zero momentum by $\simeq 162 \text{ MeV}$.

Fig. 6 shows the momentum dependence of the K^+ potential. Again the dashed line indicates our calculations using the K^+p forward scattering amplitude in free space. The solid line is our result obtained when excluding the low energy solution from Martin [32]. The crossed rectangle in Fig. 6 shows the result of Ref. [12] extracted from the K^+ production data at $\theta_{lab} = 44^\circ$ in $Ni + Ni$ collisions at 0.8, 1.0 and 1.8 A·GeV [7] and in $Au + Au$ collisions at 1 A·GeV [8]. The calculations within the quark-meson coupling model [39] predict an increase of the K^+ -meson mass at ρ_0 and zero antikaon momentum by $+ 24 \text{ MeV}$, which is in reasonable agreement with our result from the dispersion relation.

Fig. 7, furthermore, shows the in-medium correction to the K^\pm -meson mass at ρ_0 again. All notations are similar to those in Figs. 5,6. The dashed lines in Fig. 7

show our parameterizations for U^\pm , which were averaged over the Fermi momentum distribution at saturation density and read explicitly

$$U^+(\rho_B, p_K) = -167 \rho_B \quad (20)$$

$$U^-(\rho_B, p_K) = -\rho_B \{341 + 823 \exp(-2.5p_K)\} \quad (21)$$

with the baryon density given in fm^{-3} and U^\pm in MeV.

4 Analysis of data from KEK

Antikaon production in proton-nucleus collisions is well suited for the extraction of the momentum dependence of the K^- -meson mass in nuclear matter because the laboratory K^\pm momenta are relative to the target system which is practically at rest. Thus, in principle, by measuring the K^\pm -meson spectrum from $p + A$ collisions one can actually probe the momentum dependence of the K^\pm potential. According to our studies in Section 3 antikaons of low momenta should see strong attractive potentials in the nucleus whereas kaons with large momenta should only see a slightly attractive potential.

Recently, the K^- -meson production in $p + C$ and $p + Cu$ collisions at a beam energy of 3.5 and 4 GeV was studied at KEK [18] where the differential K^- production cross section was measured at an emission angle of 5.1° in the laboratory and at a momentum $p_K = 1.5 \text{ GeV}/c$. In order to test the sensitivity of the experimental data to the in-medium K^\pm mass we have performed calculations within the coupled channel transport approach HSD used in Refs. [10, 12] for kaon and antikaon production in nucleus-nucleus collisions, in Ref. [40] for ρ -meson production in $p + A$ collisions and in Ref. [41] for antiproton production in $p + A$ and $A + A$ collisions at SIS energies. We note that the local density approximation involved in the transport calculation as well as the on-shell treatment of production and absorption events might be questionable for a light nucleus such as ^{12}C , but the detailed comparison to experimental pion spectra performed in Ref. [40] and to K^+ spectra in Ref. [13] indicates that these uncertainties should be less than 30%. This systematic error (arising from the transport simulation itself) is smaller than the uncertainty in the elementary K^- production cross section in pN reactions (cf. Section 2).

Fig.8 shows the K^- spectra from $p+^{12}\text{C}$ collisions at 3.5 GeV calculated for different values of U^\pm in comparison to the experimental data point from Ref. [18] shown with both the statistical and systematical errors. Actually, at an antikaon momentum of 1.5 GeV/c one can not distinguish very well between the calculations with bare masses and e.g. $U^+=30 \text{ MeV}$ and $U^- = -60 \text{ MeV}$ as obtained in Section 3. However, it seems clear that the experimental point allows to exclude a very strong attractive K^- potential of e.g. $U^- = -240 \text{ MeV}$. On the other hand our calculations indicate a substantial change of the K^- -meson spectra due to in-medium modifications especially at low antikaon momenta.

Figs. 9,10 show our calculations for the momentum spectra of K^- -mesons from $p+C$ and $p+Cu$ collisions at the bombarding energy of 4 GeV for different values of the kaon and antikaon potential U^\pm at ρ_0 in MeV. Though the sensitivity to kaon and antikaon

potentials is less pronounced at the higher energy for both systems we may conclude that the experimental data do not contradict an in-medium modification for K^+ and K^- mesons according to the momentum-dependent K^\pm potential. Furthermore, the fast antikaons are not sensitive to the actual value of the in-medium potential U^\pm , since we do not observe sizeable differences between the calculations with bare K^+ and K^- masses and with potentials $U^+=+30$ MeV and $U^- = -60$ MeV as expected from Section 3.

On the other hand, our analysis of K^- -production with laboratory momenta of 1.5 GeV excludes a strong reduction of the antikaon mass for $U^- \leq 120$ MeV, which was found for low energy antikaons (in the cms) from heavy-ion collisions. Moreover, Figs. 8,9,10 illustrate, that in case of proton-nucleus collisions the low energy antikaons are most sensitive to in-medium effects. This effect can also be understood easily when comparing the ratio of the kaon or antikaon potential with the kaon energy at a fixed momentum. This ratio (even for momentum-independent potentials) increases with decreasing momentum. Simply due to energy conservation an antikaon seeing an attractive potential in the nucleus will be decelerated on its way to the continuum thus enhancing the spectrum at low momenta - provided that it is not absorbed in the nucleus via the reaction $K^-N \rightarrow \pi Y$, where Y denotes a hyperon.

5 Predictions for COSY energies

The in-medium change of the K^- properties can be observed through an enhancement of the production yield or, as found before, in the modification of the antikaon spectrum. Both phenomena might be studied in proton-nucleus reactions experimentally and constrain the information about the K^\pm potential in nuclear matter at normal density ρ_0 . Whereas the data points at KEK are above the threshold in free nucleon-nucleon collisions, one expects that in-medium potentials are more pronounced at subthreshold energies in $p + A$ reactions as in case of antiproton production [41].

Experiments on K^- production in $p + A$ collisions have been proposed for the proton synchrotron COSY [42]. The K^- -meson production cross section as well as the momentum spectra will be measured for bombarding energies around 2.5 GeV and kaon emission angles $\theta_{lab} \leq 10^\circ$. In these experiments a rather precise measurement of the K^- -meson spectra can be performed, which might allow to reconstruct the antikaon potential up to momenta of 1.3 GeV/c [43]. The K^- -meson production threshold in NN collisions in free space corresponds to a proton beam energy of $\simeq 2.5$ GeV and the experiments at COSY aim at the near or subthreshold physics. Actually the cross section for subthreshold K^- production in proton-nucleus collisions is small but the reaction threshold might drop due to the decrease of the in-medium antikaon mass [13].

Fig. 11 shows the K^- production cross section integrated over all antikaon momenta from $p + {}^{12}\text{C}$ collisions as a function of the bombarding energy. The lines indicate our calculations with bare K^\pm masses and for the separate contributions from the direct pN and secondary πN production channel. For the K^- -meson production from secondary πN interactions we show the calculations using only the exclusive $\pi N \rightarrow NKK^-$ channel (dotted line) as well as the inclusive $\pi N \rightarrow K^-X$ reaction channels as illustrated in Fig. 1. Note, that while at KEK energies the contributions from the direct and

secondary K^- production mechanism are approximately the same, at COSY energies the secondary reaction channels are dominant. In Fig. 11 we also indicate the proton beam energy corresponding to the absolute threshold for the antikaon production in $p + C$ collisions, which is available for the coherent process $pC \rightarrow pCKK^-$.

Fig. 12, furthermore, shows the calculated momentum spectrum for K^- -mesons produced in $p+^{12}C$ and $p+^{207}Pb$ collisions at the proton beam energy of 2.5 GeV. The spectrum is integrated over the K^- emission angle up to $\theta_{lab} = 10^\circ$, which corresponds to the experimental setup of the COSY-ANKE detector. The solid histograms (b) show our calculation with bare masses for both kaon and antikaon. The dotted histograms (a) show the calculations with bare masses when neglecting the final state absorption of K^- -mesons. It is clear that FSI have a very strong effect on the antikaon spectrum. K^- absorption gives roughly a factor of 2 reduction in cross section for ^{12}C while it amounts to a factor ≈ 5 for ^{207}Pb . The dashed histograms (c) indicate our results obtained with in-medium potentials $U^+ = 30$ and $U^- = -120$ MeV and taking into account the FSI. In the latter case the absolute K^- -meson production cross section substantially increases and the spectrum is shifted to lower momenta as noted before.

We conclude that the shape of the K^- spectrum as well as the absolute value of the production cross section from proton-nucleus collisions are very sensitive to the magnitude of the K^\pm potential in the baryonic matter and should be determined experimentally by comparing the spectra from light and heavy targets as a function of momentum.

6 Conclusions

We have calculated the momentum dependence of the K^+ and K^- -meson potentials based on dispersion relations for the $K^\pm N$ forward scattering amplitude at finite nuclear density. We have found that the in-medium K^+ potential almost does not depend on the kaon momentum and increases to $\simeq +30$ MeV at nuclear matter density $\rho_B = 0.17 \text{ fm}^{-3}$. The K^- potential drops to $\simeq -200$ MeV at zero antikaon momentum and saturates at ≈ -60 MeV at high momenta. Our results are in reasonable agreement with the in-medium potentials evaluated from the measurement of kaonic atoms [5], as well as from the previous studies [9, 10, 12] on K^\pm -production from heavy-ion collisions [6, 7, 8].

Furthermore, we have analysed the recent data from KEK [18] on antikaon production in proton-nucleus collisions at bombarding energies of 3.5 and 4 GeV. The data do not contradict our results for the momentum dependent K^\pm potential, however, the experimental results are not very sensitive to the actual magnitude of the in-medium masses at the high momentum of 1.5 GeV. On the other hand, we have illustrated that $p + A$ reactions at COSY for bombarding energies close to the threshold in proton-proton collisions might be well suited for the evaluation of the K^\pm potential in nuclear matter (at ρ_0) as a function of the antikaon momentum in the laboratory.

Appendix

The total cross section for the K^+p reaction can be parametrized as a function of the kaon momentum p_K in the laboratory system as

$$\begin{aligned} \sigma &= 12.4 & p_K &\leq 0.78 \\ \sigma &= 1.09 + 14.5 p_K & 0.78 < p_K &\leq 1.17 \\ \sigma &= 18.64 - 0.5 p_K & 1.17 < p_K &\leq 2.92 \end{aligned} \quad (23)$$

where the cross section is given in mb and the kaon momentum p_K in GeV/c . At higher momenta we use the Regge parametrization from Donnachie and Landshoff [44]. Fig. 13 illustrates the comparison between our parametrization and the experimental data [20].

The total K^-p cross section is parametrized as

$$\begin{aligned} \sigma &= 26.32/p_K & p_K &\leq 0.25 \\ \sigma &= 36.4 p_K^{-0.26} & 1.81 < p_K &\leq 3 \\ \sigma &= 32.25 p_K^{-0.15} & 3 < p_K &\leq 17 \end{aligned} \quad (24)$$

In the antikaon momentum range from 0.25 to 1.81 GeV/c the cross section is approximated as

$$\sigma = 13.2 p_K^{-1.47} + \sum_{i=1}^4 C_i \frac{\Gamma_i^2}{(\sqrt{s} - M_i)^2 + \Gamma_i^2/4} \quad (25)$$

where the parameters C_i , Γ_i and M_i are listed in Table 1 and \sqrt{s} denotes the invariant mass of the colliding KN system. Again at high K^- momenta we use the results from Ref. [44]. Fig. 14 shows our parametrization together with the experimental data from Ref.[20].

Table 1: Parameters of the approximation (25).

| i | C_i (mb) | M_i (GeV) | Γ_i (GeV) |
|-----|------------|-------------|------------------|
| 1 | 10.4 | 1.518 | 0.012 |
| 2 | 7.6 | 1.81 | 0.17 |
| 3 | 1.8 | 1.695 | 0.05 |
| 4 | 6.4 | 2.107 | 0.37 |

References

- [1] D. B. Kaplan and A. E. Nelson, Phys. Lett. B 175 (1986) 57.
- [2] T. Waas, N. Kaiser and W. Weise, Phys. Lett. B 379 (1996) 34.
- [3] J. Schaffner-Bielich, I. N. Mishustin and J. Bondorf, Nucl. Phys. A 625 (1997) 325.
- [4] G.E. Brown and M. Rho, Phys. Rev. Lett. 66 (1991) 2720.

- [5] E. Friedman, A. Gal and C.J. Batty, Phys. Lett. B 308 (1993) 6; Nucl. Phys. A 579 (1994) 518.
- [6] A. Schröter et al., Z. Phys. A 350 (1994) 101.
- [7] R. Barth et al., Phys. Rev. Lett. 78 (1997) 4007.
- [8] P. Senger et al., Acta Phys. Pol. B 27 (1996) 2993.
- [9] G.Q. Li, C.M. Ko and X.S. Fang, Phys. Lett. B 329 (1994) 149.
- [10] W. Cassing, E.L. Bratkovskaya, U. Mosel, S. Teis and A. Sibirtsev, Nucl. Phys. A 614 (1997) 415.
- [11] G. Q. Li, C.-H. Lee, and G. E. Brown, Nucl. Phys. A 625 (1997) 372.
- [12] E.L. Bratkovskaya, W. Cassing and U. Mosel, Nucl. Phys. A 622 (1997) 593.
- [13] W. Cassing et al., Proceedings of the 8th International Conference on Nuclear Reaction Mechanisms, Varenna, June 1997, ed. by E. Gadioli, p. 142.
- [14] T. Waas, M. Rho and W. Weise, Nucl. Phys. A 617 (1997) 449.
- [15] A. Ohnishi, Y. Nara and V. Koch, Phys. Rev. C 56 (1997) 2767.
- [16] M.F.M. Lutz, nucl-th/9802033.
- [17] R. E. Chrien, R. Sawafta, R. J. Peterson, R. A. Michael, and E. V. Hungerford, Nucl. Phys. A 625 (1997) 251.
- [18] Y. Sugaya et al., sub. to Nucl. Phys. A.
- [19] A. Sibirtsev, W. Cassing and C.M. Ko, Z. Phys. A 358 (1997) 101.
- [20] Landolt-Börnstein, New Series, ed. H. Schopper, I/12 (1988).
- [21] B. Nilsson-Almqvist and E. Stenlund, Comput. Phys. Commun. 43 (1987) 387.
- [22] J.W. Waters, W.D. Walker, A.R. Erwin and J.W. Elbert, Nucl. Phys. B 17 (1976) 445.
- [23] H. Ströbele, Nucl. Phys. A 610 (1996) 102c.
- [24] G.E. Brown, Phys. Bl. 53 (1997) 671.
- [25] D. Amati, Phys. Rev. 113 (1959) 1692
- [26] R. Perrin and W.S. Woolcock, Nucl. Phys. B4 (1968) 671.
- [27] N.M. Queen, Nucl. Phys. B1 (1967) 207.
- [28] P. Bailon et al., Phys. Let. 50B (1974) 383

- [29] R.E. Hendrick and B. Lautrup, Phys. Rev. D11 (1975) 529.
- [30] B.R. Martin and M. Sakitt, Phys. Rev. 183 (1969) 1345.
- [31] J.K. Kim, Phys. Rev. Lett. 14 (1965) 29; 19 (1967) 1079.
- [32] A.D. Martin, Nucl. Phys. B 16 (1970) 479; B 179 (1981) 33.
- [33] D.J. Miller, Los Alamos Nat. Lab., Physics With LAMPF (1984) 213.
- [34] R.C. Barrett, Nuovo Cim. 102 A (1989) 179.
- [35] O.V. Dumbrajs, T.Yu. Dumbrajs and N.M. Queen, Fortschr. Phys. 19 (1971) 491.
- [36] N.M. Quin, M. Restignoli and G. Violini, Fortschr. Phys. 17 (1969) 467
- [37] O.V. Dumbrajs, T.Yu. Dumbrajs and N.M. Queen, Nucl. Phys. B 26 (1971) 497.
- [38] G. Brown and M. Rho, Nucl. Phys. A 596 (1996) 503.
- [39] K. Tsushima, K. Saito, A.W. Thomas and S. Wright, nucl-th/9712044.
- [40] A. Sibirtsev and W. Cassing, Nucl. Phys A 629 (1998) 717.
- [41] A. Sibirtsev, W. Cassing, G. I. Lykasov, and M. V. Ryzjanin, Nucl. Phys. A 632 (1998) 131.
- [42] T. Kirchner et al., COSY Proposal 21.
- [43] A. Sibirtsev, M. Büscher, H. Müller and Ch. Schneidereit, Z. Phys. A 351 (1995) 333.
- [44] A. Donnachie and P.V. Landshoff, Phys. Lett. B 296 (1992) 227.

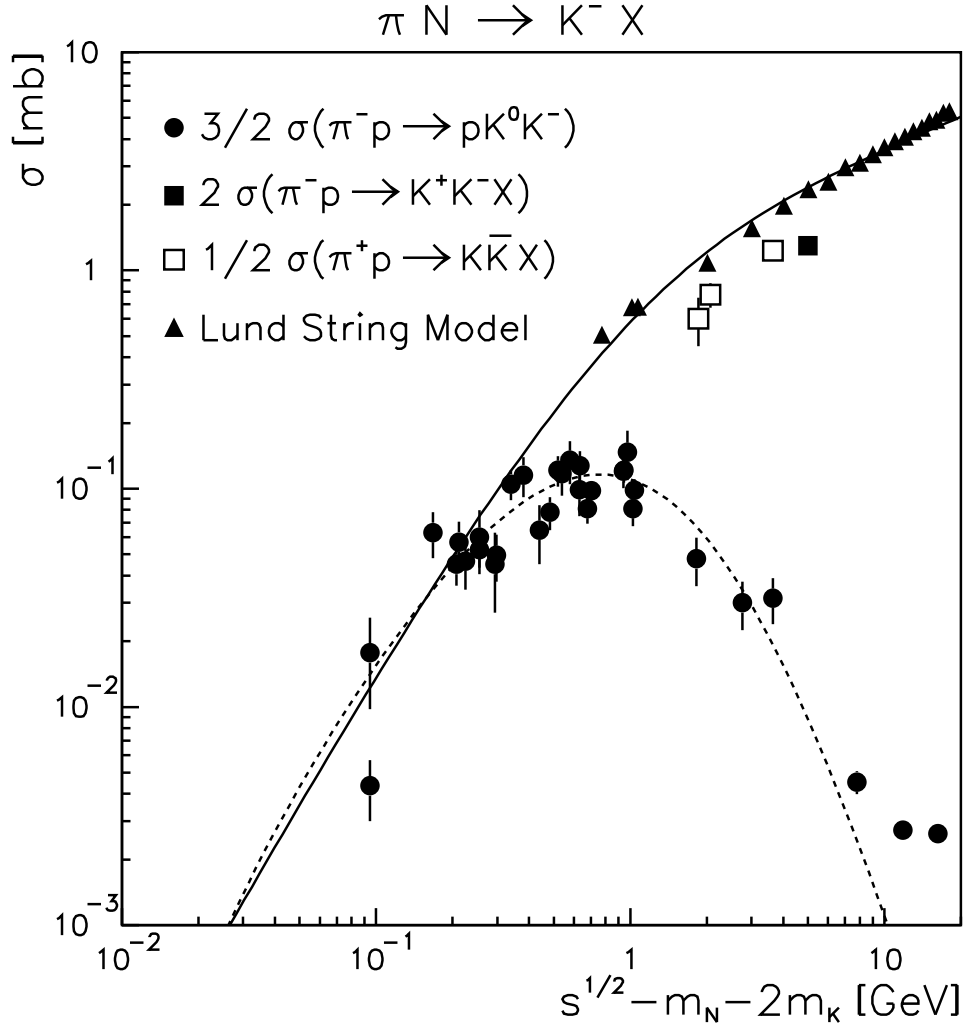


Figure 1: The K^- -production cross section from πN collisions as a function of the excess energy $\epsilon = \sqrt{s} - m_N - 2m_K$ above the $\pi N \rightarrow NK\bar{K}$ reaction threshold. The dashed line shows the exclusive cross section from Ref. [19] while the solid line is our parametrization for the inclusive K^- -production; the triangles show the calculations within the Lund-string-model (LSM) at higher energy while the experimental data (full dots and open squares) are taken from Ref. [20].

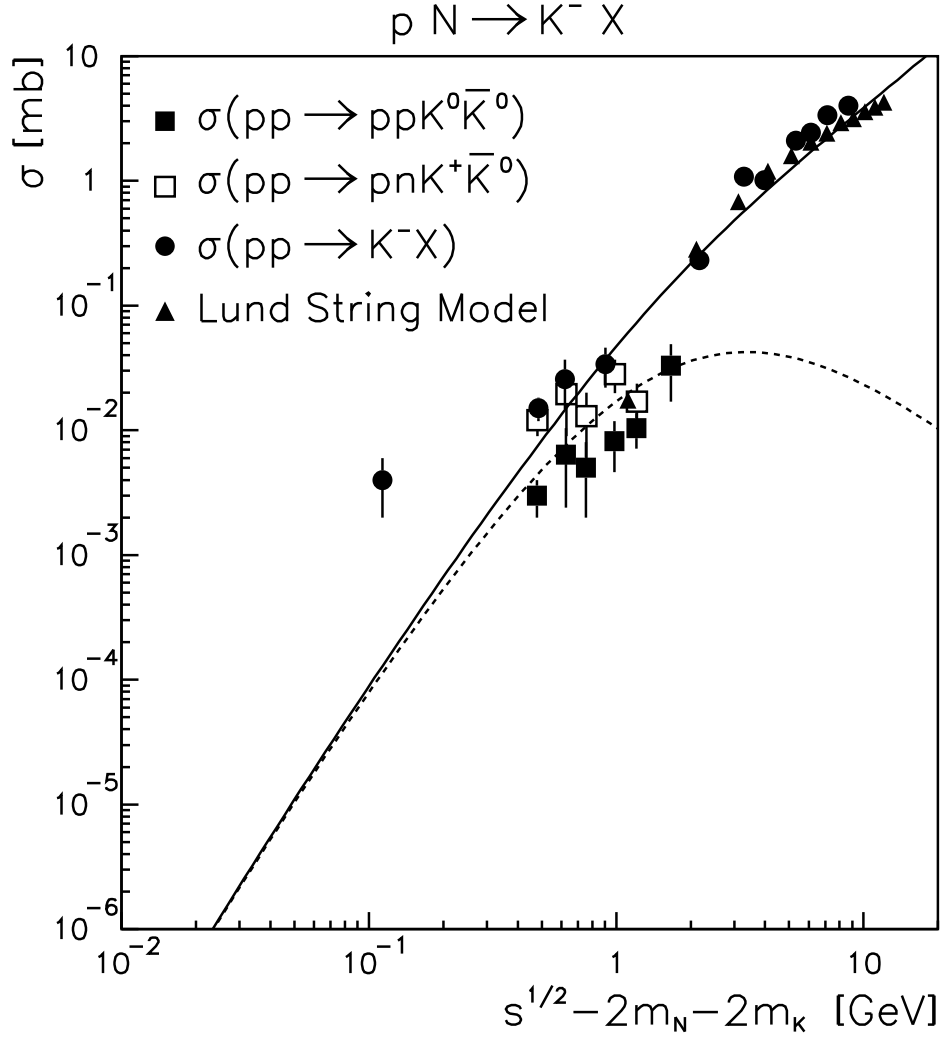


Figure 2: The cross section for K^- -production in pN collisions as a function of the excess energy above the $NN \rightarrow NNK\bar{K}$ reaction threshold. The dashed line shows the exclusive cross section calculated within the OBEM [19] while the solid line is our parametrization for the inclusive K^- -production cross section. The triangles show the calculations within the LSM in comparison to the experimental data (full dots) taken from Ref. [20].

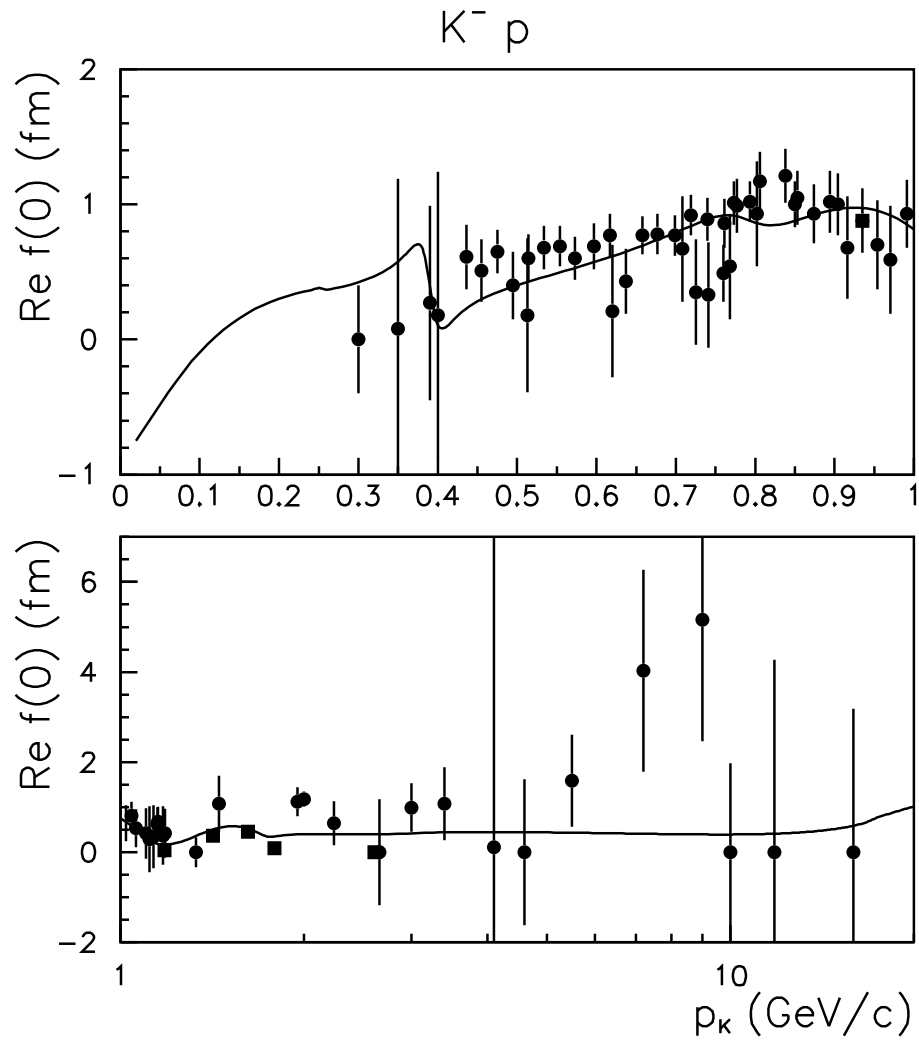


Figure 3: Real part of the K^-p scattering amplitude (solid line) in comparison to the experimental data taken from Ref. [35].

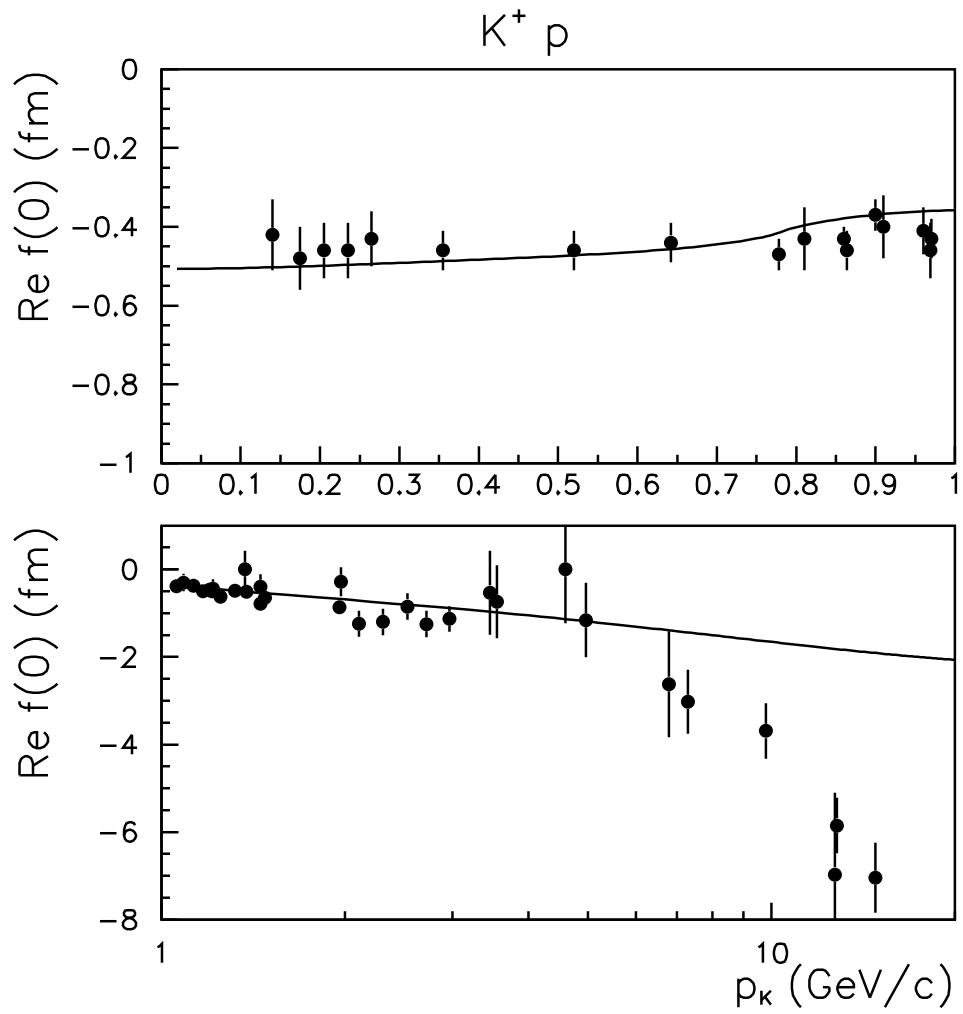


Figure 4: Real part of the K^+p scattering amplitude (solid line) in comparison to the experimental data taken from Ref. [35].

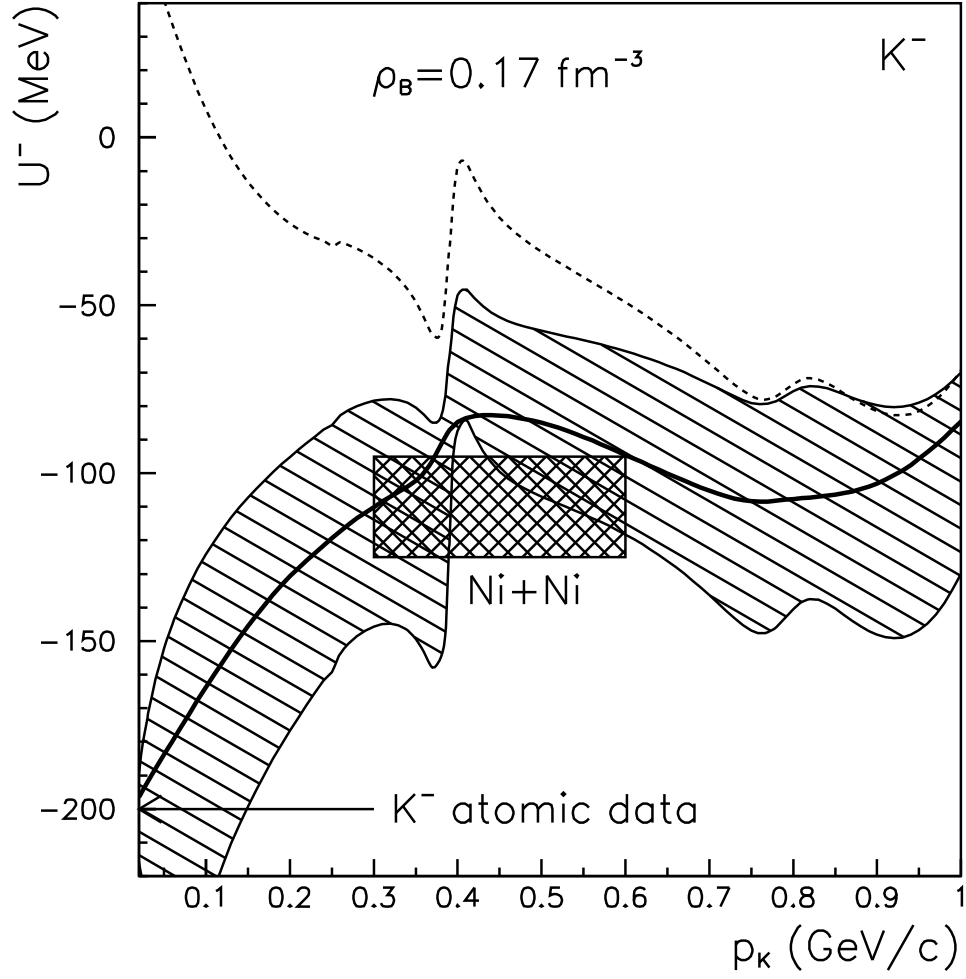


Figure 5: The K^- potential at nuclear saturation density as a function of the antikaon momentum p_K . The dashed line shows the calculations with the vacuum K^-p scattering amplitude; the fat solid line is our result excluding the $\Sigma(1385)$ and $\Lambda(1405)$ resonances while the lined area indicates the uncertainty of our calculations. The arrow shows the result from the K^- atomic data [5] whereas the crossed rectangle indicates the results from the analysis of K^- production in $Ni + Ni$ collisions [10, 9].

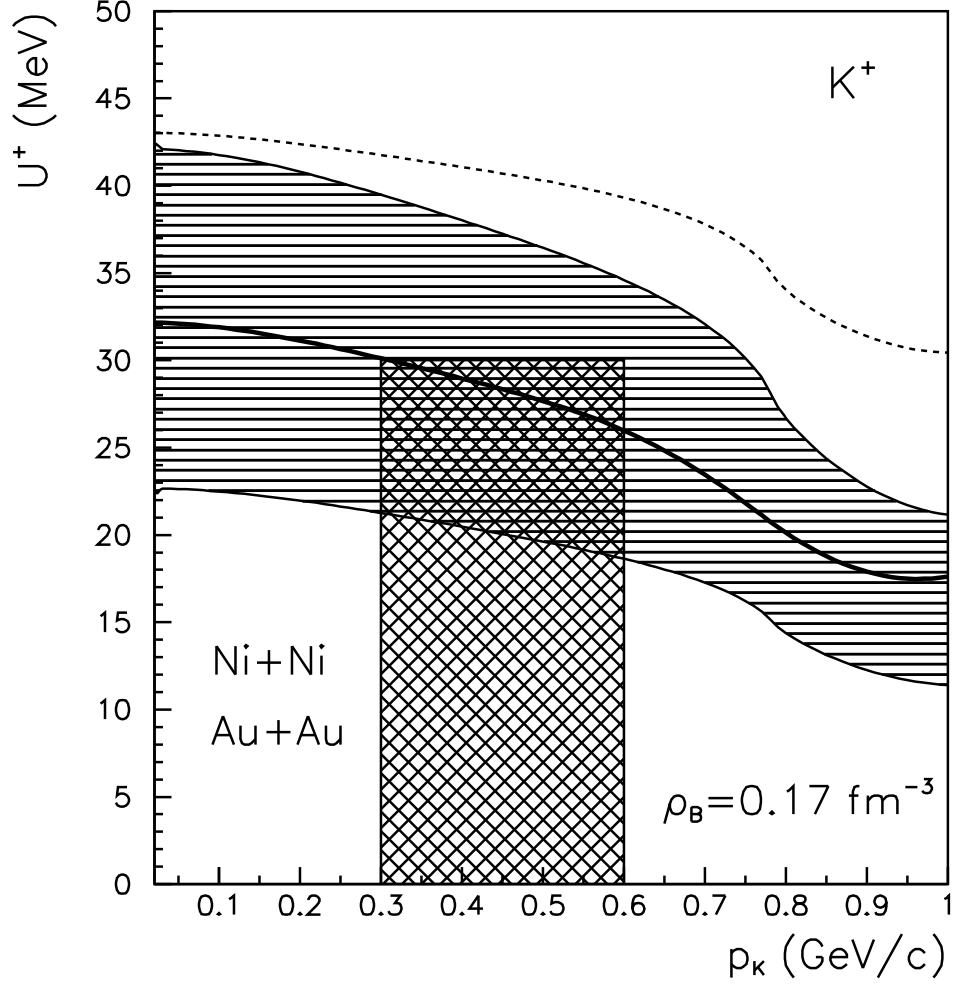


Figure 6: The K^+ potential at nuclear saturation density as a function of the kaon momentum. The dashed line shows the calculation with the vacuum K^+p scattering amplitude while the fat solid line is our result obtained by excluding the $\Sigma(1385)$ and $\Lambda(1405)$ resonances. The lined area demonstrates the uncertainty of our calculations. The crossed rectangle shows the results from the analysis of K^+ production in $Ni + Ni$ and $Au + Au$ collisions at SIS energies [12].

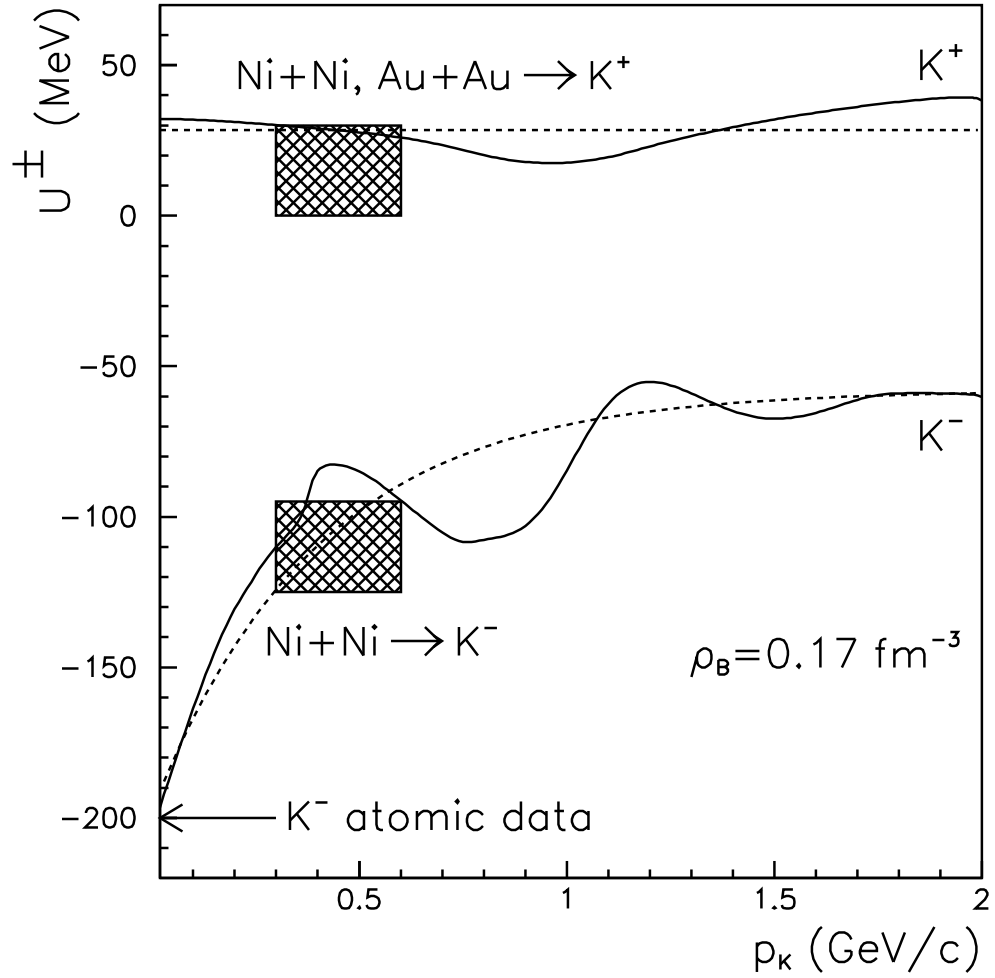


Figure 7: The K^\pm potential at nuclear saturation density as a function of the kaon momentum. The dashed lines show our parameterization for the Fermi averaged potentials. The other notations are the same as in Figs.5,6.

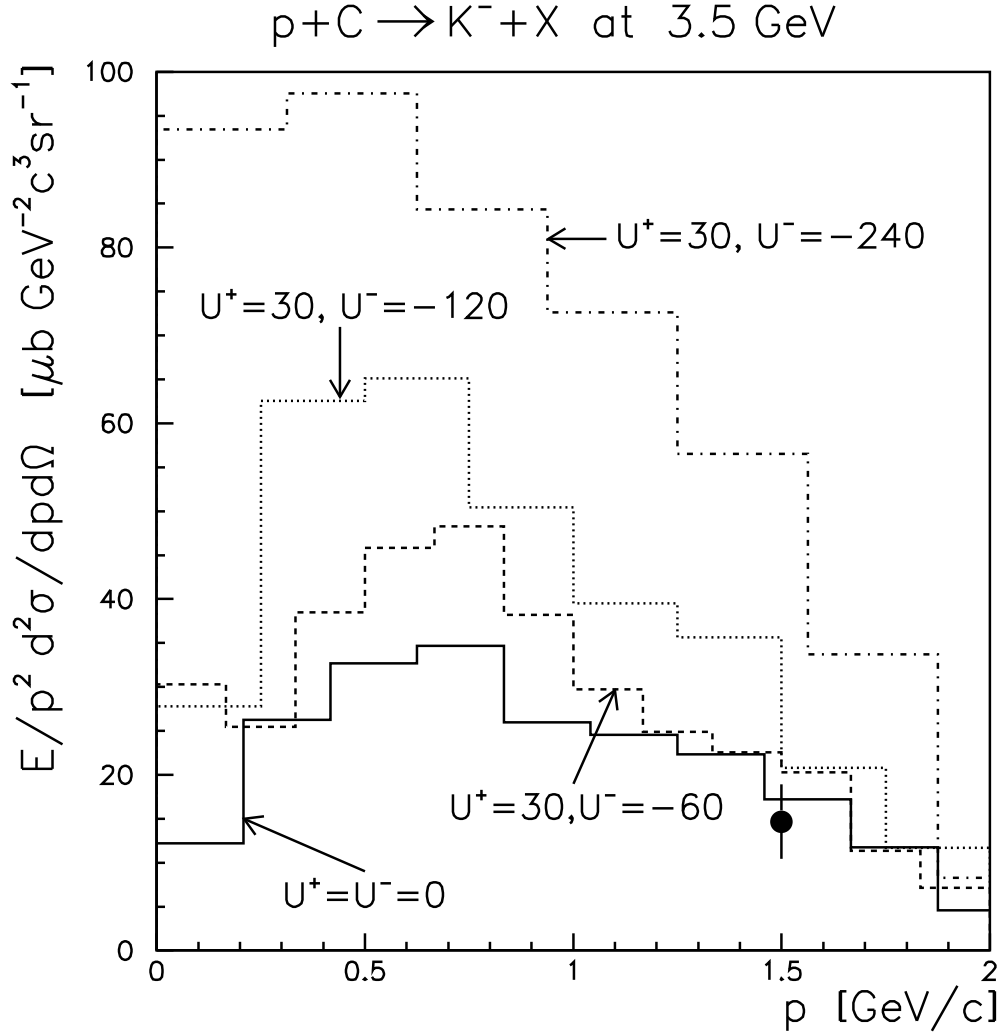


Figure 8: Momentum spectra of K^- -mesons from $p + {}^{12}\text{C}$ collisions at a bombarding energy of 3.5 GeV and laboratory angle $\theta_{lab} = 5^\circ$ calculated for different in-medium potentials for kaons U^+ and antikaons U^- in MeV. The experimental point is taken from Ref. [18] and shown with the systematical error.

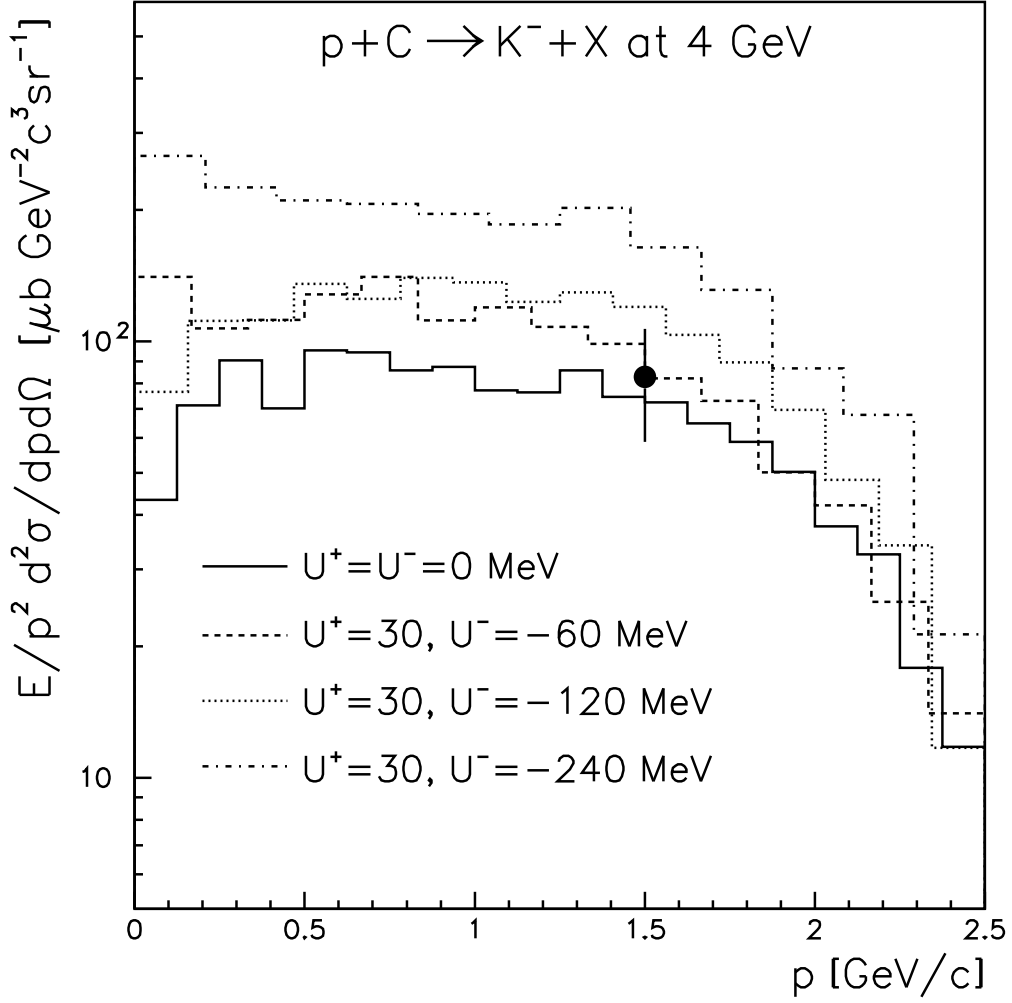


Figure 9: The momentum spectra of K^- -mesons from $p+C$ collisions at the bombarding energy of 4 GeV. The histograms show our calculations with different in-medium potentials for kaons U^+ and antikaons U^- in MeV. The experimental point is taken from Ref. [18] and shown with the systematical error.

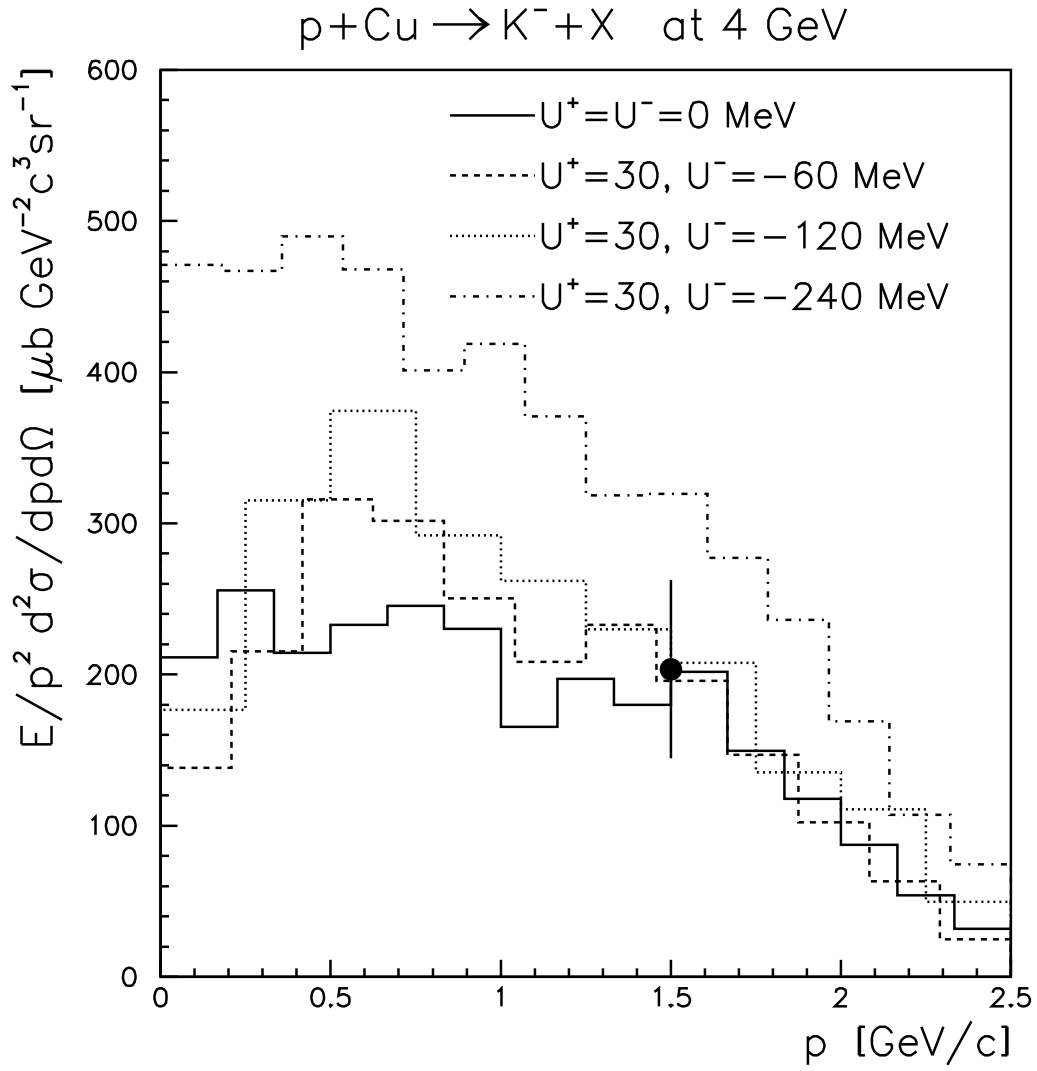


Figure 10: The momentum spectra of K^- -mesons from $p + Cu$ collisions at the bombarding energy of 4 GeV. The histograms show our calculations with different in-medium potentials for kaons U^+ and antikaons U^- while the full dot indicates the experimental data point from Ref. [18].

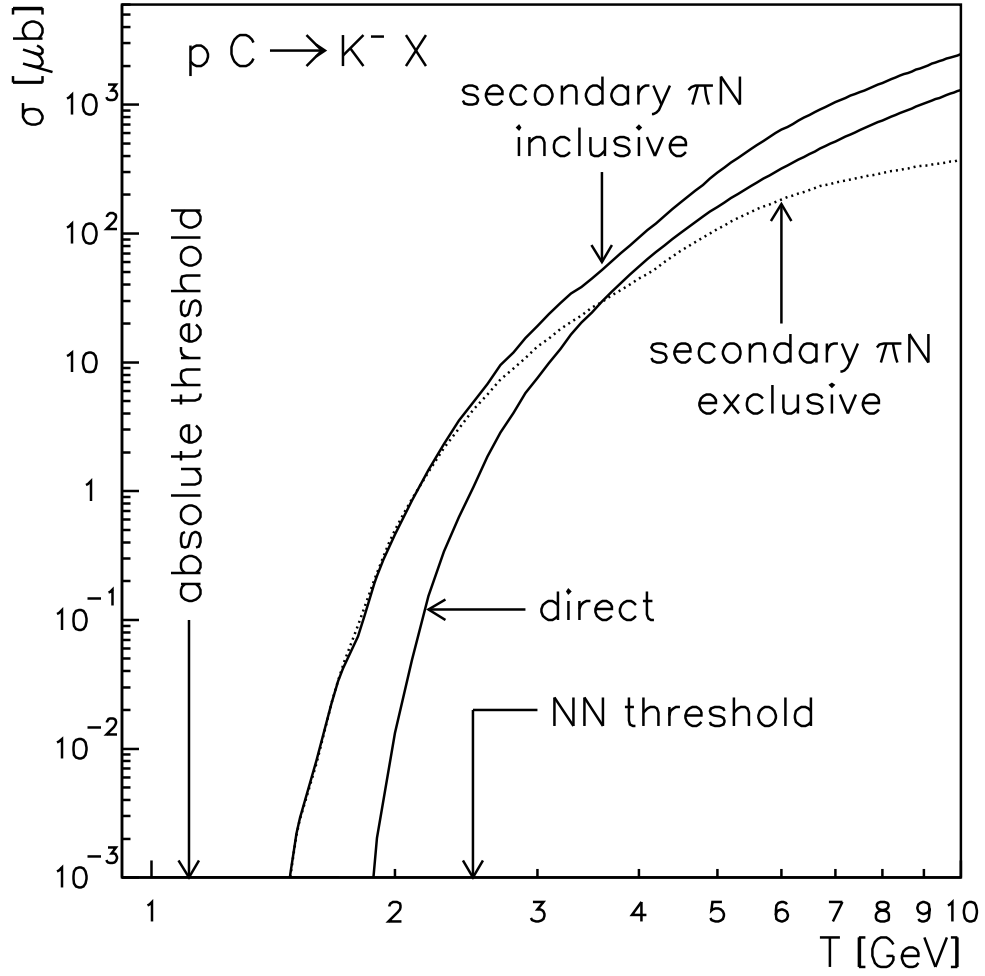


Figure 11: The cross section for K^- production in $p + {}^{12}\text{C}$ collisions as a function of the bombarding energy using bare kaon and antikaon masses. The lines show our calculations for the direct (pN) and secondary (πN) production mechanisms. The arrows indicate the absolute and NN reaction threshold, respectively.

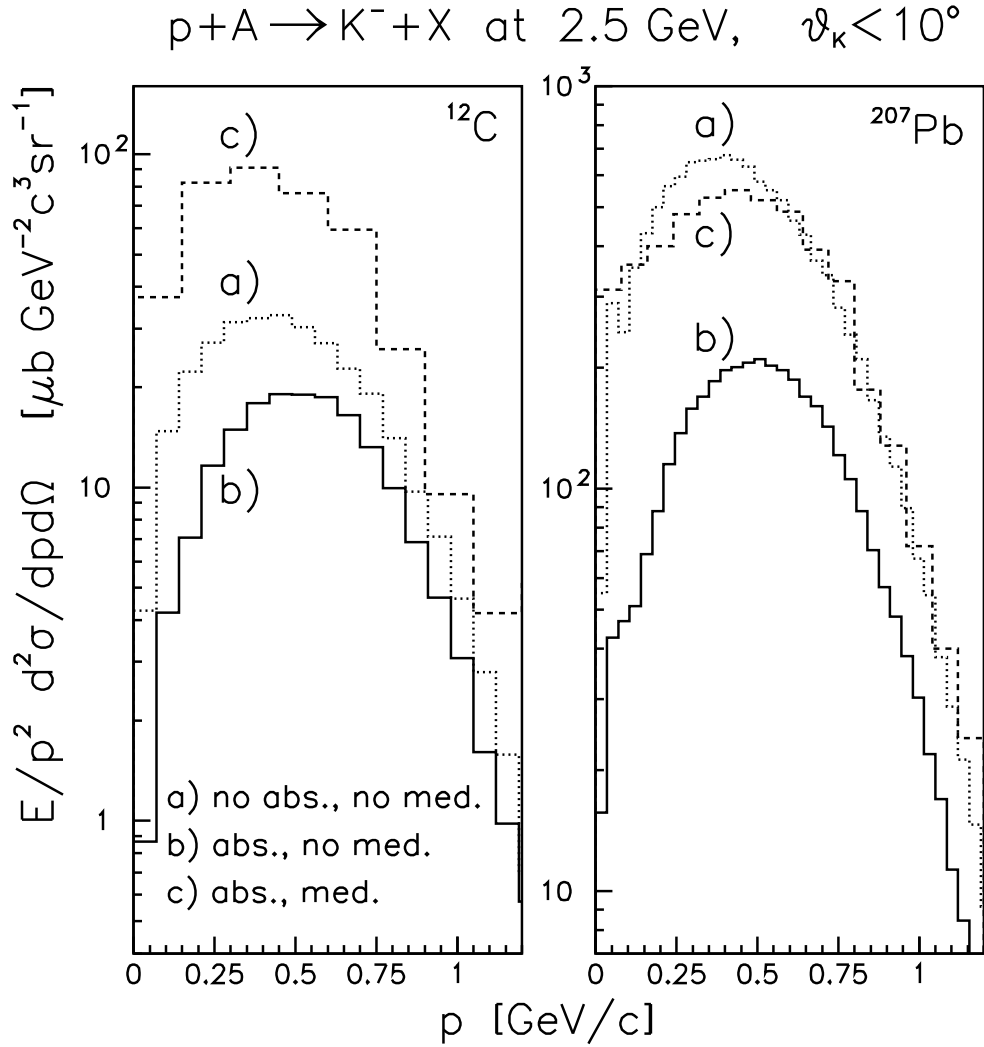


Figure 12: The K^- spectrum from $p + {}^{12}\text{C}$ and $p + {}^{207}\text{Pb}$ collisions at 2.5 GeV for antikaon emission angles $\leq 10^\circ$. The solid histograms show our calculations with bare masses and K^- absorption (b), the dotted histograms are calculated with bare masses and without absorption (a) while the dashed histogram is our result for in-medium potentials of K^+ ($U^+ = 30$ MeV) and K^- ($U^- = -120$ MeV) mesons and with K^- absorption (c).

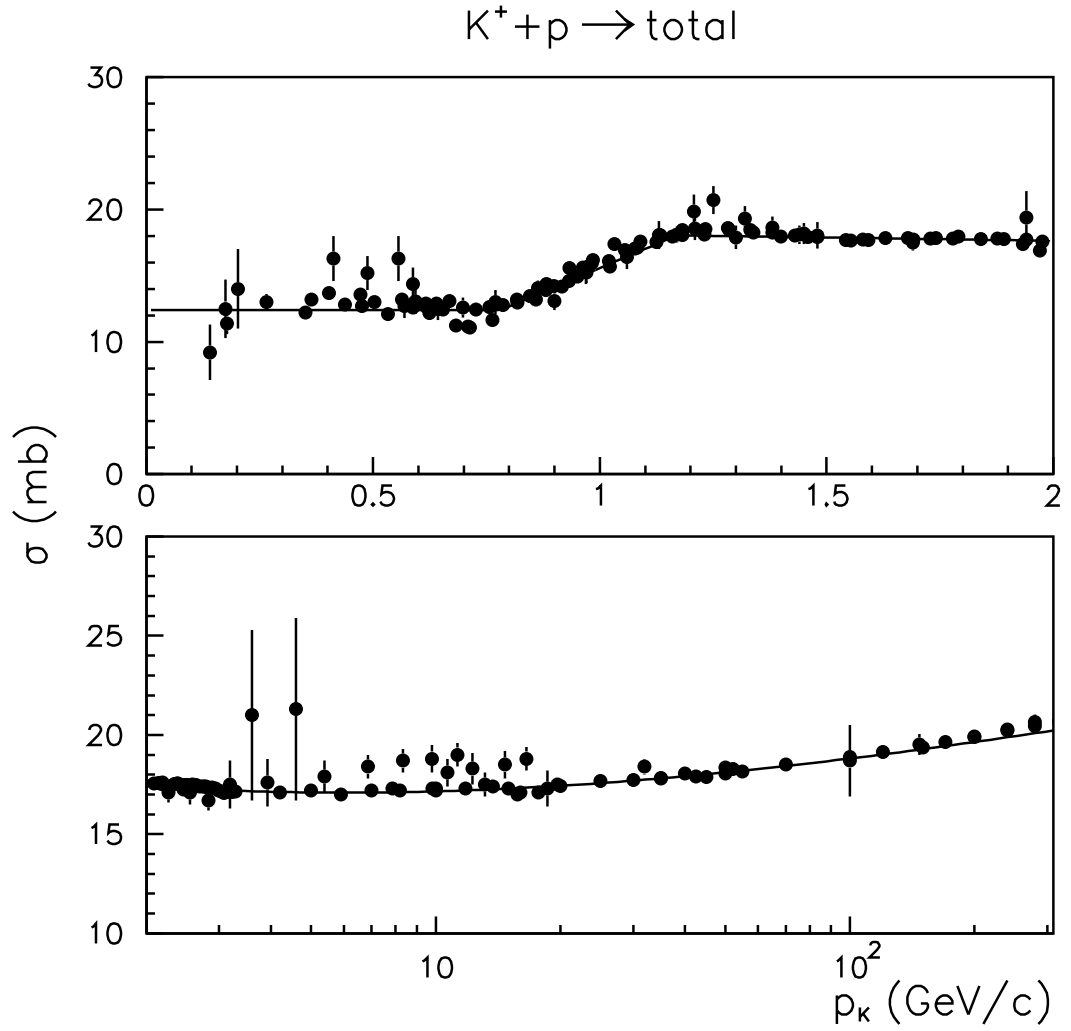


Figure 13: Total K^+p cross section as a function of the kaon momentum in the laboratory frame. The experimental data are taken from Ref. [20] while the lines show our parametrization.

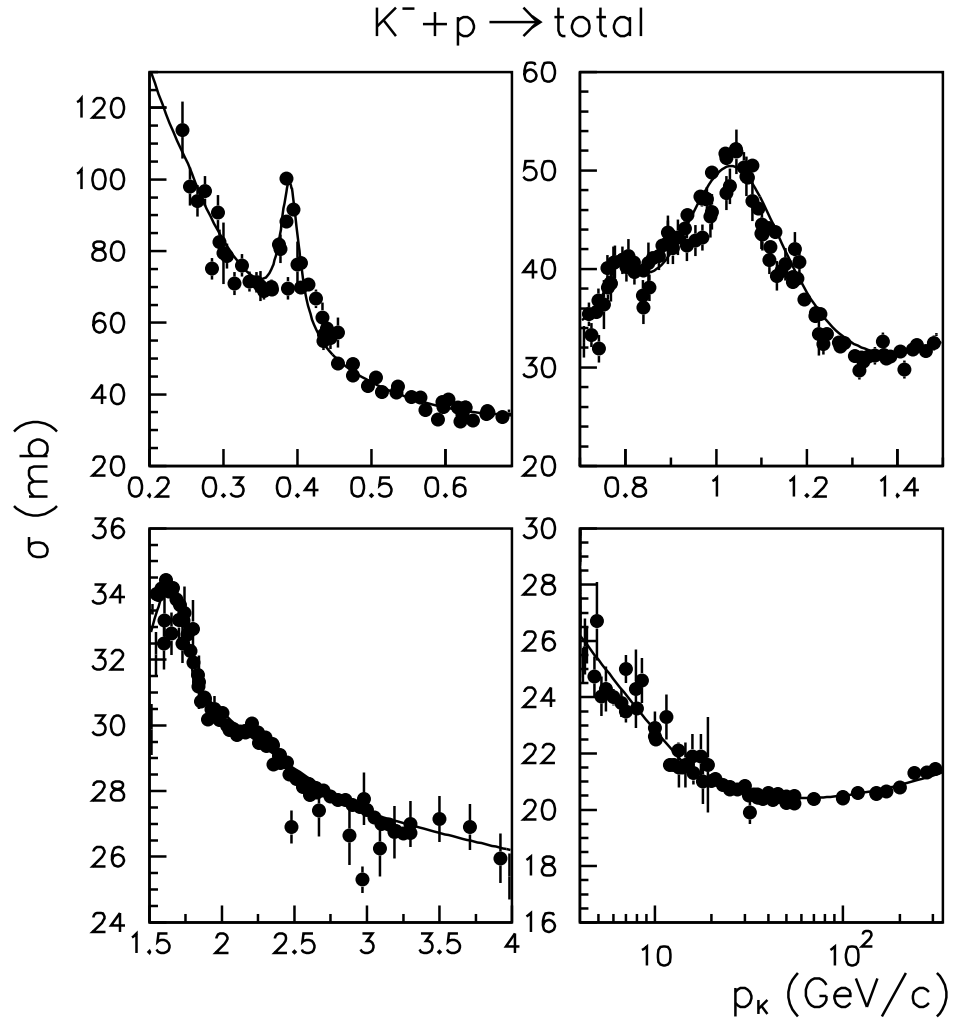


Figure 14: Total K^-p cross section as a function of the kaon momentum in the laboratory frame. The experimental data are taken from Ref. [20] while the lines show our parametrization.